

Contents

1 Theory	3
1.1 Sesquioxides	3
1.1.1 Chromium Oxide	4
1.1.2 Gallium Oxide	6
1.2 X-ray Diffraction Principles	8
1.2.1 Scattering at Lattices	8
1.2.2 X-rays	9
1.3 Heteroepitaxy	10
1.3.1 Pseudomorphic Growth	10
1.3.2 Relaxed Growth	12
Dislocations	12
Slip Systems for Sesquioxide Heterostructures	13
2 Experimental Methods	15
2.1 Pulsed Laser Deposition	15
2.1.1 Setup	16
2.1.2 Plasma Dynamics	16
2.1.3 Segmented Target Approach	18
2.2 X-Ray Diffraction Measurement	18
2.2.1 2θ - ω -scans	19
2.2.2 ω -scans	20
2.2.3 φ -scans	21
2.2.4 Reciprocal Space Maps	21
2.2.5 Technical Aspects	24
2.3 Further Methods	24
2.3.1 Thermal Evaporation	24
2.3.2 Resistivity Measurement	25
2.3.3 Thickness Determination	26
2.3.4 Spectral Transmission	27
3 Experiment, Results and Discussion	29
3.1 Preliminary Investigations	30
3.1.1 Experiment	30
3.1.2 Results	30
Oxygen Partial Pressure Variation on <i>m</i> -plane Sapphire	30
Growth Temperature Variation on <i>m</i> -plane Sapphire	32
Influence of Growth Rate on Crystal Structure	35

	Deposition on <i>c</i> -, <i>r</i> -, <i>m</i> - and <i>a</i> -plane Sapphire	37
3.1.3	Conclusion	39
3.2	Doping of Cr ₂ O ₃ Thin Films	41
3.2.1	Experiment	41
3.2.2	Results	42
	Laser Position Variation for Different Targets	42
	Ohmic Contact Optimization	49
3.2.3	Conclusion	49
3.3	Strain Analysis	51
3.3.1	Experiment	51
	Sample Fabrication	51
	Measurements	52
3.3.2	Results	54
	<i>c</i> -plane: Laser Spot Size Variation	56
	<i>c</i> -plane: Pulse Energy Variation	58
	<i>r</i> -plane: Laser Spot Size Variation	60
	<i>r</i> -plane: Pulse Energy Variation	61
	<i>m</i> - and <i>a</i> -plane: Laser Spot Size Variation	63
	<i>m</i> - and <i>a</i> -plane: Pulse Energy Variation	64
3.3.3	Conclusion	67
3.4	Cr ₂ O ₃ Buffer Layers for Rhombohedral Ga ₂ O ₃	69
3.4.1	Experiment	69
3.4.2	Results	70
3.4.3	Conclusion	74
	Appendices	75
	A Calculations	77
A.1	<i>m</i> -plane lattice constants	77
A.2	<i>a</i> -plane lattice constants	78
	B Figures	79
	Bibliography	85

Chapter 3

Experiment, Results and Discussion

Contents

3.1	Preliminary Investigations	30
3.1.1	Experiment	30
3.1.2	Results	30
3.1.3	Conclusion	39
3.2	Doping of Cr₂O₃ Thin Films	41
3.2.1	Experiment	41
3.2.2	Results	42
3.2.3	Conclusion	49
3.3	Strain Analysis	51
3.3.1	Experiment	51
3.3.2	Results	54
3.3.3	Conclusion	67
3.4	Cr₂O₃ Buffer Layers for Rhombohedral Ga₂O₃	69
3.4.1	Experiment	69
3.4.2	Results	70
3.4.3	Conclusion	74

3.4 Cr_2O_3 Buffer Layers for Rhombohedral Ga_2O_3

A major motivation for investigating Cr_2O_3 thin films is due to a possible usage as buffer layer for $\alpha\text{-}\text{Ga}_2\text{O}_3$, which has similar lattice parameters. This could improve the crystal quality of the latter due to reduced lattice mismatch when compared to Al_2O_3 [1]. From Fig. 3.33 it becomes clear that Cr_2O_3 has a larger c lattice constant, but a smaller a lattice constant than $\alpha\text{-}\text{Ga}_2\text{O}_3$. Therefore, e.g., the in-plane compressive strain observed for c -plane Cr_2O_3 thin films actually further decreases the mismatch between Cr_2O_3 and $\alpha\text{-}\text{Ga}_2\text{O}_3$. For m -plane samples, however, the in-plane compressive strain yields a larger discrepancy between the a lattice constant of both sesquioxides. In the following, a proof of concept will be given that $\alpha\text{-}\text{Ga}_2\text{O}_3$ can successfully be deposited on Cr_2O_3 buffer layers.

3.4.1 Experiment

For the Cr_2O_3 thin films, deposition parameters were chosen that yielded the lowest strain and ω -FWHM. Therefore, a lens position of -1 cm and a laser pulse energy of 450 mJ were applied. Note that 350 mJ would result in even better crystallinity, but only at the cost of very low growth rates. The Ga_2O_3 layer was deposited with a lens position of -1 cm and a laser pulse energy of 650 mJ . This is the configuration that was used for depositing Cr_2O_3 in 3.1 and 3.2. By assuming a growth rate of 10 pm pulse^{-1} – which is achieved for deposition with similar parameters at a different PLD chamber –, $15\,000$ pulses were applied to achieve a layer thickness of 150 nm . The oxygen partial pressure was $3 \times 10^{-4}\text{ mbar}$ and the temperature was chosen to be approx. ??. Two approaches were chosen to deposit $\alpha\text{-}\text{Ga}_2\text{O}_3$ of four different orientations c , r , m and a :

1. Deposition of Cr_2O_3 with subsequent analysis of the Cr_2O_3 layer under atmospheric conditions. Afterwards the Ga_2O_3 layer was deposited *ex situ* in a distinct PLD process.
2. *In situ* deposition of Cr_2O_3 and Ga_2O_3 without returning to atmospheric conditions inbetween. Between both processes, the oxygen pressure was reduced and it was waited for 20 min to achieve thermodynamic equilibrium.

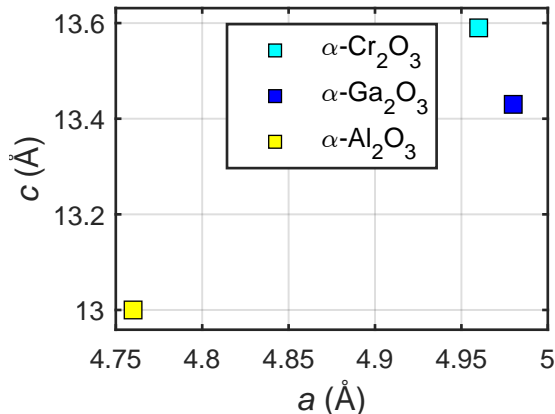


Figure 3.33: Lattice constants a and c for the three sesquioxides relevant in this work.

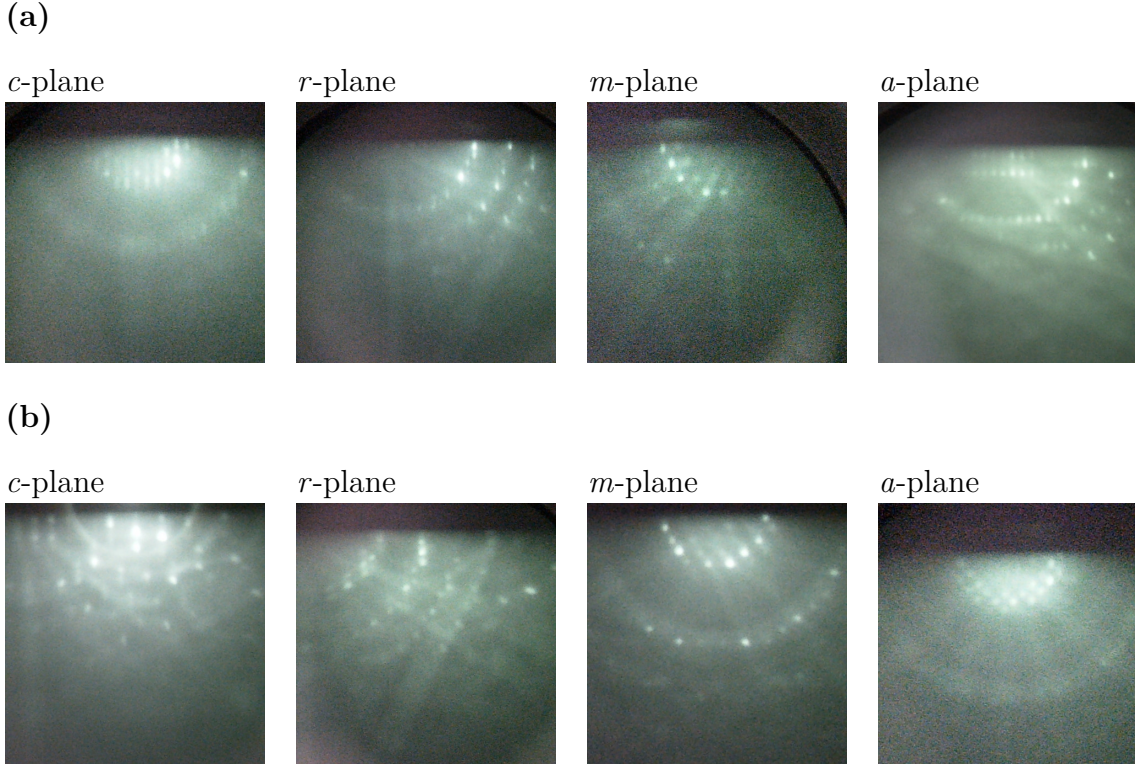


Figure 3.34: RHEED patterns of the α - Ga_2O_3 surface deposited (a) *ex situ* on Cr_2O_3 and (b) *in situ* on Cr_2O_3 . Note that the patterns were recorded in arbitrary azimuth which is why they may differ between *ex situ* and *in situ* deposition. This is not necessarily a result of different crystal structure.

For the *ex situ* samples, Reciprocal Space Maps (RSMs) were recorded before and after the deposition of the Ga_2O_3 layer. For all samples, 2θ - ω -scans were performed in the range of 10 to 130° after deposition of the Ga_2O_3 layer. Furthermore, Reflection High-Energy Electron Diffraction (RHEED) patterns were recorded for the surfaces of all samples after deposition of the Ga_2O_3 layer. RHEED is a method to probe the crystal structure of only a few monolayers below the surface of a thin film. High-energy electrons are pointed in grazing incidence geometry on the sample surface and the diffracted electrons are detected with a florescent screen. The image of the screen is called the RHEED pattern and it can yield information about the symmetry and crystallinity of the sample surface [2].

The 2θ - ω patterns are compared to a reference Cr_2O_3 sample, namely sample A from 3.3, which was also fabricated with a pulse energy of 450 mJ. The theoretical predictions of the 2θ values for reflections of β - Ga_2O_3 were taken from the *Materials Project* [3, mp-886].

3.4.2 Results

The RHEED patterns of all samples from the *ex situ* and *in situ* batch are depicted in Fig. 3.34a and Fig. 3.34b, respectively. From the periodic patterns it can be concluded that every surface is crystalline. Note that the mere observation of crystallinity does not indicate which phase of Ga_2O_3 is present on the samples.

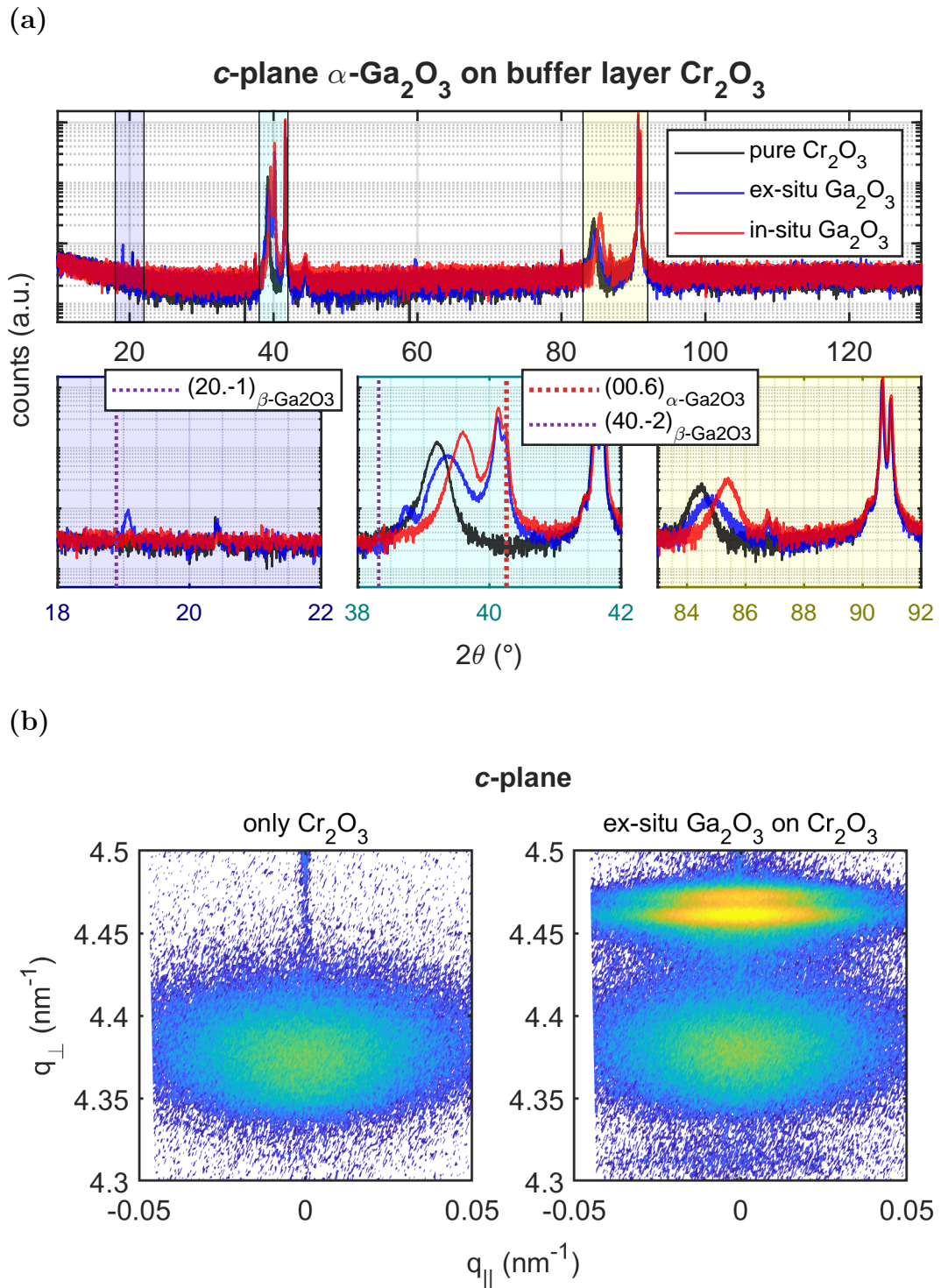


Figure 3.35: (a) $2\theta\text{-}\omega$ -patterns of the *c*-plane Cr_2O_3 reference sample A (black), as well as the *ex situ* (blue) and *in situ* (red) buffer layer structures. (b) RSM around the $(00,6)$ reflection recorded before (left) and after (right) *ex situ* deposition of Ga_2O_3 on Cr_2O_3 .

Table 3.4: Selected reflections of β -Ga₂O₃ and their predicted positions in 2θ - ω patterns as well as their relative intensities. Data taken from Ref. [3, mp-886]

2 θ	reflection	relative intensity
18.89°	(20 $\bar{1}$)	8.7
38.3°	(31 $\bar{1}$)	57.0
38.32°	(40 $\bar{2}$)	3.6
38.36°	(202)	2.5

In Fig. 3.35a, 2θ - ω patterns are depicted of the Cr₂O₃ reference sample A (black), as well as of the *ex situ* (blue) and *in situ* (red) samples. The peak at around 39.2° of the reference sample is the (00.6) reflection of Cr₂O₃. This reflection is also attributed to the peaks at approx. 39.4° and 39.6° of the *ex situ* and *in situ* samples, respectively. The variation of peak position for the Cr₂O₃ layer may originate in the fact that for each process, the thickness may have varied which was determined to be a crucial factor for the out-of-plane strain. Despite this peak, two overlaying peaks occur at 40.14° for both buffer layer processes. This is attributed to the (00.6) reflection of α -Ga₂O₃, because the predicted peak position is at 40.26° with a relative intensity⁽¹⁴⁾ of 3.37, and is therefore allowed. The presence of two peaks is attributed to the splitting between Cu-K α_1 and Cu-K α_2 radiation (*K α splitting*). Note that at approx. 86°, the higher order (00.12) reflection of Cr₂O₃ can be observed more dominantly than the (00.12) reflection of α -Ga₂O₃. This is due to the fact the the ratio of relative intensities of (00.12) to (00.6) is 29.6 % for Cr₂O₃ and only 1.4 % for α -Ga₂O₃.

For the *in situ* sample, no additional peaks are observed, indicating phase-pure deposition of *c*-plane Ga₂O₃ in the α -phase on *c*-plane Al₂O₃. For the *ex situ* sample, however, a peak occurs at 38.71° and the β -phase of Ga₂O₃ has three different predicted peaks at this position, listed in Tab. 3.4. The observed peak is attributed to the (40 $\bar{2}$) reflection, because at 19.06°, another peak is observed that can only correspond to the (20 $\bar{1}$) reflection of β -Ga₂O₃ (Tab. 3.4), which favors the identification of (40 $\bar{2}$) as a higher order reflection. Note that the peak observed at 20.4° is also observed for the Cr₂O₃ reference sample and can therefore not correspond to any Ga₂O₃ phase.

In Fig. 3.35b, the RSMs of the *ex situ* sample are displayed. Note that the image is cropped such that no substrate peak is visible. The previous result is confirmed that another phase has formed on top of the Cr₂O₃ layer. No ω -scans were done, but the crystallinity can be estimated by the broadening in $q_{||}$ direction, which is less dominant in comparison to the Cr₂O₃ layer. Furthermore, the K α splitting indicates a highly crystalline thin film.

The 2θ - ω patterns of the *r*-plane reference and buffer layer samples are depicted in Fig. 3.36a. Due to very close peak positions of the (02.4) reflection for both Cr₂O₃ and α -Ga₂O₃, a comparison with the reference sample is not as straightforward as for the other orientations. No additional peak can be identified for the buffer layer samples. However, the RHEED patterns indicated a crystalline surface, which is why the only possible phase of the Ga₂O₃ layer is the α -phase. This is verified by RSMs of the *ex*

⁽¹⁴⁾ This value indicates the peak intensity of a reflection in powder diffraction patterns and gives a hint to identify peaks.

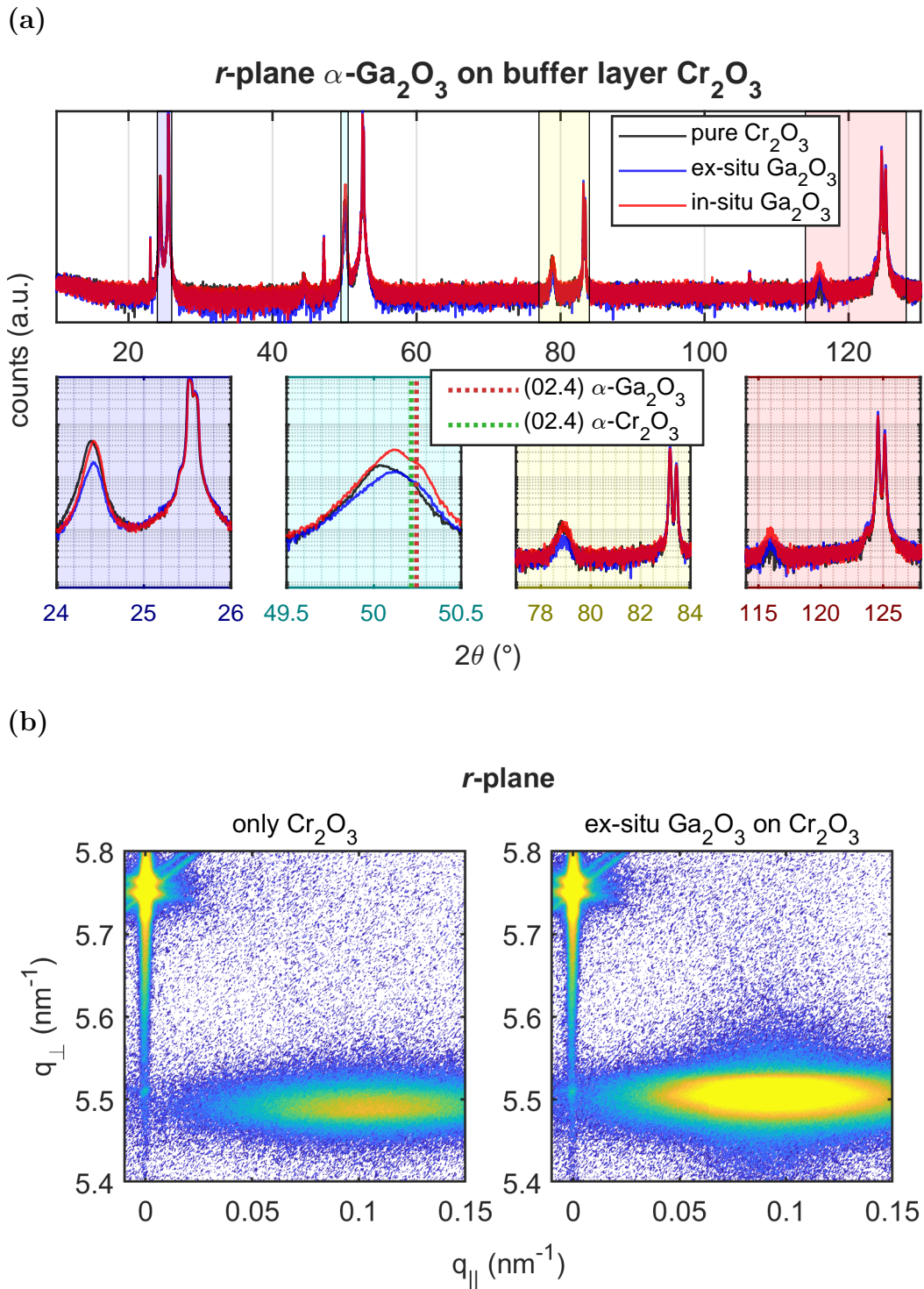


Figure 3.36: (a) $2\theta\text{-}\omega$ -patterns of the r -plane Cr_2O_3 reference sample A (black), as well as the *ex situ* (blue) and *in situ* (red) buffer layer structures. (b) RSM around the (02.4) reflection recorded before (left) and after (right) *ex situ* deposition of Ga_2O_3 .

situ sample in Fig. 3.36b: a significant increment in intensity can be observed at the expected peak position of (02.4) α -Ga₂O₃, which is due to the formation of α -phase Ga₂O₃ on *r*-plane Cr₂O₃.

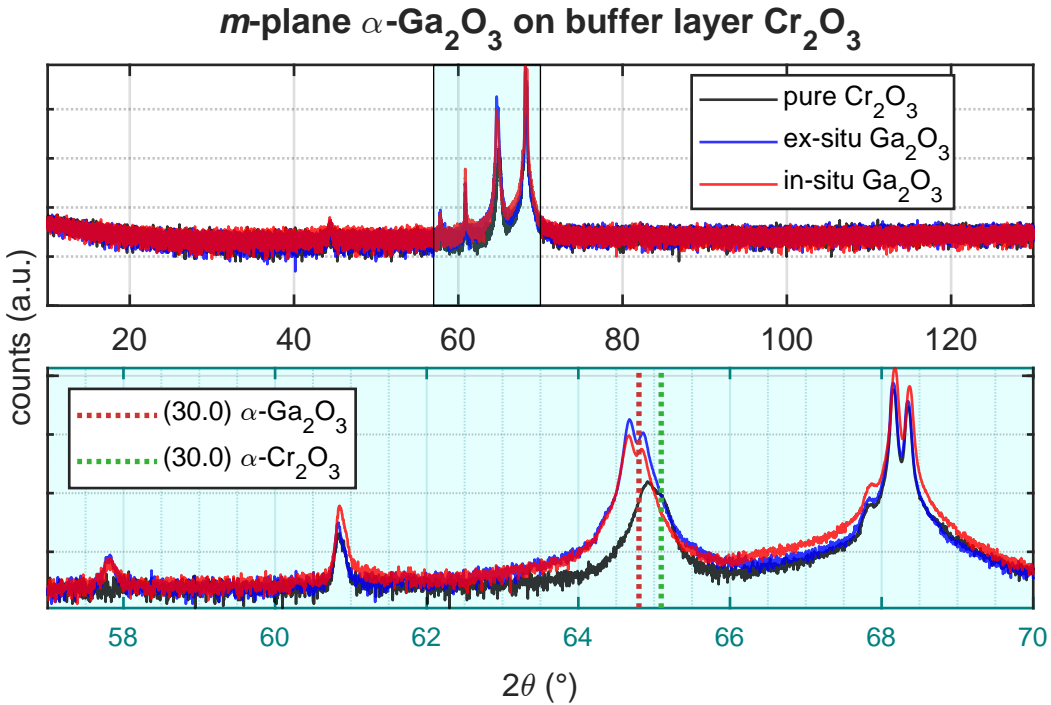
When comparing the peaks of *m*-plane buffer layer samples to the Cr₂O₃ reference sample, note that the (30.0) peak is shifted to lower angles (Fig. 3.37a). Furthermore, two peaks can be observed for the buffer layer samples, which may originate in (i) either two peaks for Cr₂O₃ and α -Ga₂O₃ each; or (ii) K α splitting of a (30.0) α -Ga₂O₃ reflection on top of the Cr₂O₃ layer. Both explanations are favored by the fact that the expected peak position (red dotted line) lays inbetween both peaks. The theoretical predictions of the 2 θ positions also have similar distance as the two peaks observed (red and green dotted lines), favoring the first explanation. However, when considering Fig. 3.37b, it becomes clear that the origin is a K α splitting, because prior to the deposition of Ga₂O₃, none of the peaks was present with the observed intensity. Therefore, the observed peaks must both stem from the α -phase of Ga₂O₃. No other peaks are observed in the 2 θ - ω pattern, therefore a phase pure α -phase is present.

A similar behavior as for the *m*-plane samples can be observed in the 2 θ - ω patterns of *a*-plane samples (Fig. 3.38a). The splitted peak is attributed to the (22.0) reflection of an α -Ga₂O₃ layer and the peak on the left shoulder to the (22.0) reflection of Cr₂O₃, which is shifted to lower angles in comparison to the reference sample. This behavior is also observed for the (11.0) reflections of both α -Ga₂O₃ and Cr₂O₃. This result is confirmed by the RSMs (Fig. 3.38b), where two peaks appear due to K α splitting after Ga₂O₃ deposition. The low broadening in q_{\parallel} direction as well as the K α splitting indicate good crystal quality.

3.4.3 Conclusion

Phase-pure depositon of α -Ga₂O₃ on Cr₂O₃ thin films was achieved for *c*-, *r*-, *m*- and *a*-plane oriented Al₂O₃ substrates. The orientation of both Cr₂O₃ and α -Ga₂O₃ thin film was the same as the respective substrate. For *ex situ* deposition of Ga₂O₃, X-ray diffraction (XRD) measurements indicate the presence of the β -phase of Ga₂O₃, which is less dominant as the still remaining α -phase. No optimization was performed for the deposition process, but the results serve as a proof of concept, that the deposition of phase-pure α -Ga₂O₃ – especially in the *c*- and *r*-orientation – is possible on Cr₂O₃ buffer layers.

(a)



(b)

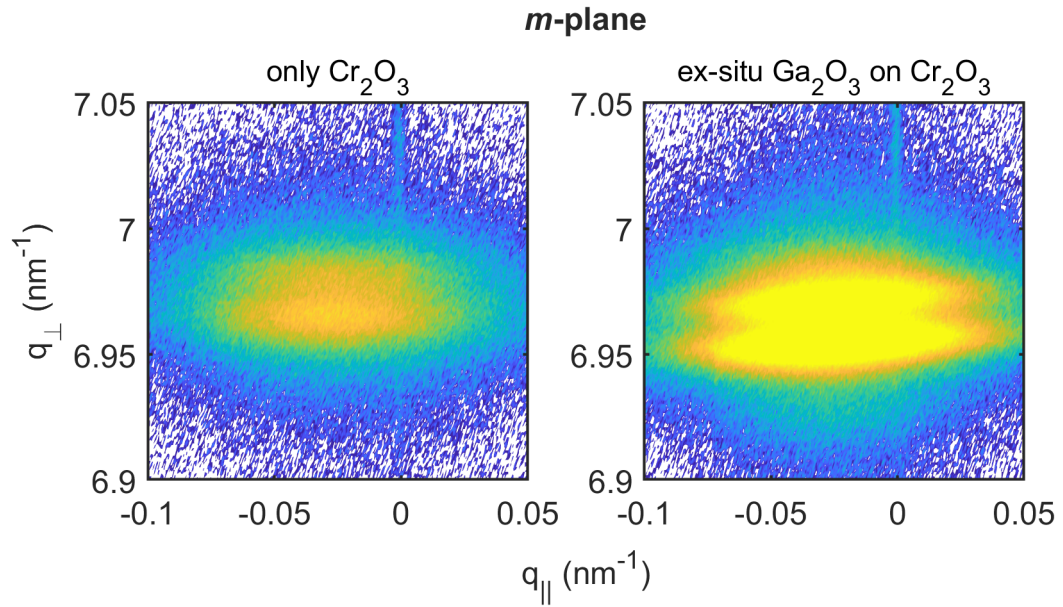


Figure 3.37: (a) $2\theta\text{-}\omega$ -patterns of the *m*-plane Cr_2O_3 reference sample A (black), as well as the *ex situ* (blue) and *in situ* (red) buffer layer structures. (b) RSM around the (30.0) reflection recorded before (left) and after (right) *ex situ* deposition of Ga_2O_3 on Cr_2O_3 .

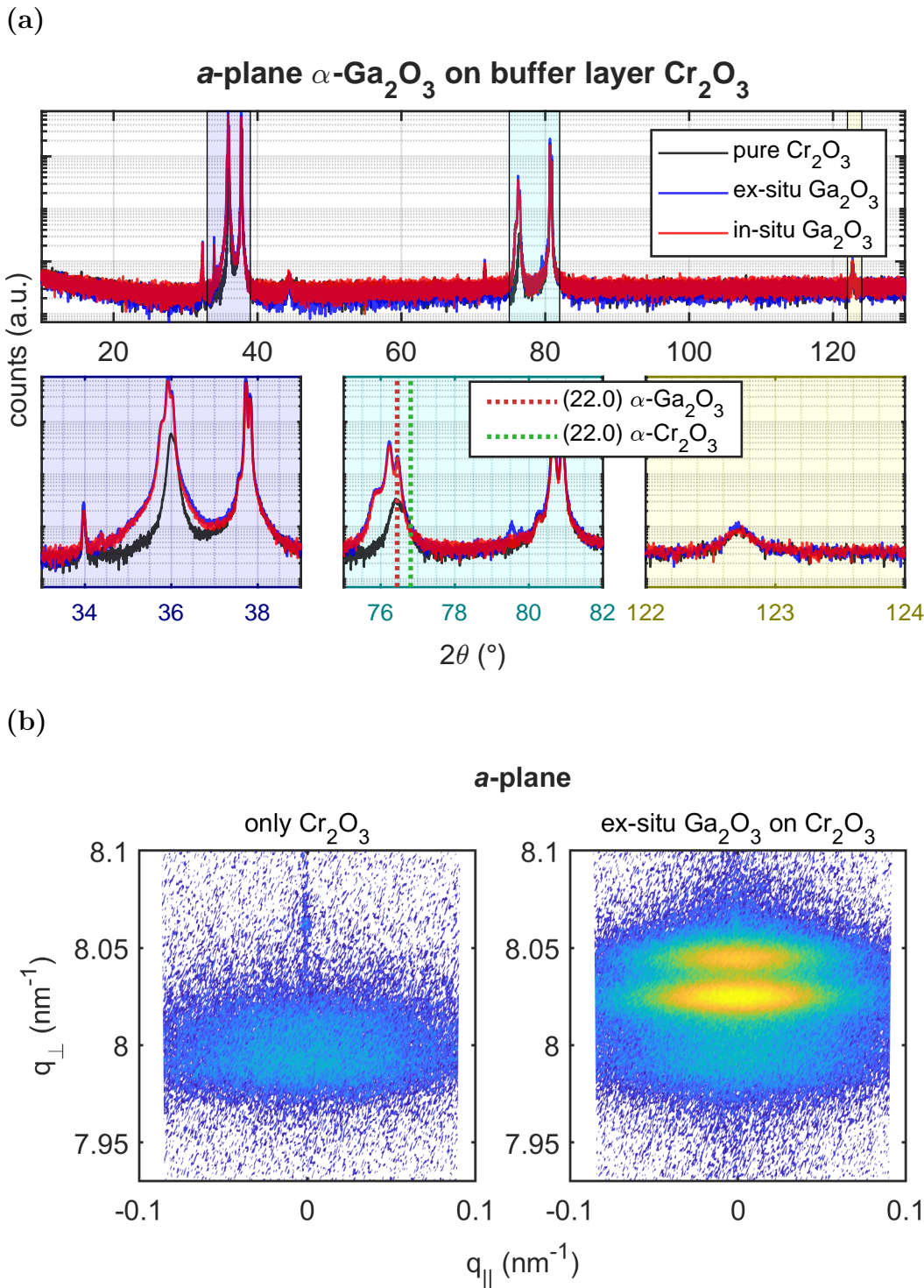


Figure 3.38: (a) $2\theta\text{-}\omega$ -patterns of the *a*-plane Cr_2O_3 reference sample A (black), as well as the *ex situ* (blue) and *in situ* (red) buffer layer structures. (b) RSM around the (22.0) reflection recorded before (left) and after (right) *ex situ* deposition of Ga_2O_3 on Cr_2O_3 .

Bibliography

- [1] S.I. Stepanov *et al.* “HVPE growth of corundum-structured α -Ga₂O₃ on sapphire substrates with α -Cr₂O₃ buffer layer”. In: *Materials Physics and Mechanics* 47 (2021), pp. 577–581. doi: [10.18149/MPM.4742021_4](https://doi.org/10.18149/MPM.4742021_4).
- [2] Mohamed A. Hafez, Mohamed K. Zayed, and Hani E. Elsayed-Ali. “Review: Geometric interpretation of reflection and transmission RHEED patterns”. In: *Micron* 159 (2022), p. 103286. ISSN: 09684328. doi: [10.1016/j.micron.2022.103286](https://doi.org/10.1016/j.micron.2022.103286).
- [3] Anubhav Jain *et al.* “Commentary: The Materials Project: A materials genome approach to accelerating materials innovation”. In: *APL Materials* 1.1 (2013), p. 011002. ISSN: 2166-532X. doi: [10.1063/1.4812323](https://doi.org/10.1063/1.4812323).